Fail-safe Control Strategy of Traction Motor in Electric Mobility with Sensorless Control Scheme

Ilhan Kim, Hyeongsu Kim, Taesuk Kwon, Hyeoundong Lee
Electric Drive Engineering Team
Hyundai Mobis
Mabuk-Ro, Yongin-Si, Korea

***Abstract* —A motor in electric mobility is utilized Eco-friendly vehicles for traction usually. The rotor position is critical factor in motor drive area. If the sensing of rotor position is fail due to potential faults, eco-friendly vehicles are uncontrollable by a driver. This paper proposes a novel sensorless algorithm to estimate the rotor position of interior permanent magnet synchronous motor (IPMSM). The algorithm is used to control vehicle by a fail-safe logic and it can be applied the continuous operation of vehicle, when the sensing of position is fail. This algorithm is comprised of two methods that can be applied in entire speed region. The first is the extended EMF method that uses the extended EMF model with the information of position error. The method is applied to the mid-high speed region of rotor. The second is the high-frequency injection method that estimates the rotor position using the injected high-frequency voltage signal. This method is applied to low-speed region which include zero speed, because there is no EMF or the magnitude of EMF is very small. Finally, the algorithm in this paper is utilized the two explained kinds of method and is verified by experimental results.**

Keywords - Inverter; Interior Permanent Magnet Synchronous Motor; Position Sensor; Sensorless Algorithm; Fail-Safe Logic

I. INTRODUCTION

The purpose of this paper is the design and implementation of the novel sensorless control algorithm against potential faults occurring in a position sensor with an application in interior permanent magnet synchronous motors (IPMSMs) employed for the traction purpose of eco-friendly vehicles. For automotive use, the sensorless control algorithm is essentially designed expecting possible advances in the motor drive's fail-safe control.

The most widely accepted sensorless control algorithms can be the EMF method with reference model proposed by Matsui [1], as well as the extended EMF method suggested by Morimoto [2][3]. These algorithms have already been commercialized for the development of industrial products with their advantages; one of them is their applicability to DSPs with fixed-point since the motor model equations used in such algorithms can be simply represented in discretized form. In contrast, their fatal disadvantage is the inaccuracy in terms of the appreciable difference between an estimated and a real rotor position, particularly at a low-speed region including a zero-speed, since the EMF on which these algorithms utterly depend is essentially based on a rotor speed.

This paper proposes the novel sensorless control algorithm exploiting two complementary control schemes in order to apply an entire speed regions, uncompromising the accuracy in a rotor position. In addition to the normal extended EMF method widely covering mid and high-speed regions, the high frequency injection method [4] is particularly devised for the problem low-speed region. The suggested control algorithm is verified by sequential experiments, and can be used to entire speed regions. Finally, the suggested algorithm in this paper is useful the motor drive area of eco-friendly vehicles with fail-safe logic.

II. THE PROPOSED SENSORLESS ALGORITHM

The proposed sensorless algorithm is used two methods depending on the rotor speed. This is the combined sensorless control method which uses the extended EMF method in mid-high speed region and the high-frequency injection method in low-speed region including zero speed. The transition between two methods in Session I progress smoothly, because a hysteresis level is utilized at the determined EMF voltage magnitude. Also, the proposed method must estimate the initial rotor position (θ_M) and magnetic polarity during the uncertain condition of position sensor fault at the initial operating step.

A. The Extended EMF Method

The rotating vectors in the stationary reference frame are described in Fig. 1. The α-axis and β-axis are defined the stationary reference frame. The d-axis and q-axis components correspond to flux and torque producing components in the rotor reference frame, respectively. Also, the γ-axis and δ-axis are the estimate of d-axis and q-axis with the sensorless algorithm.

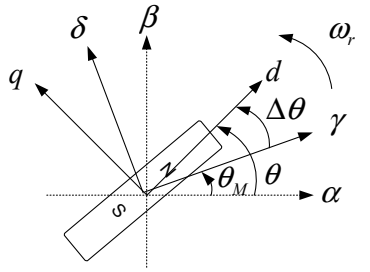

Figure 1. Rotating vector in the stationary reference frame

978-1-4673-0990-5/12/$31.00 ©2012 IEEE

The EMF method has the unclear equations in the process of approximation; therefore the extended EMF method is modified on the conventional method [1]. This is clearer than the conventional EMF method. The voltage equation for the IPMSM in the rotor reference frame can be defined in the space vector plane as Equation (1).

$$\begin{bmatrix} v_d \\ v_q \end{bmatrix} = \begin{bmatrix} R + pL_d & -\omega_r L_q \\ \omega_r L_q & R + pL_d \end{bmatrix} \begin{bmatrix} i_d \\ i_q \end{bmatrix} + \begin{bmatrix} e_{xd} \\ e_{xq} \end{bmatrix} \quad (1)$$
$$\begin{bmatrix} e_{xd} \\ e_{xq} \end{bmatrix} = \begin{bmatrix} 0 \\ (L_d - L_q)(\omega_r i_d - p i_q) + \omega_r K_E \end{bmatrix} = \begin{bmatrix} 0 \\ E_x \end{bmatrix}$$

Where,

- K_s: electromotive force coefficient
- ω_r: speed of electrical angle
- E_x: the extended EMF

Equation (2) is transformed to the voltage equation of estimated γ-axis and δ-axis using Equation (1).

$$\begin{bmatrix} v_\gamma \\ v_\delta \end{bmatrix} = \begin{bmatrix} R + pL_d & p\Delta\theta L_d - \omega_r L_q \\ p\Delta\theta L_d + \omega_r L_q & R + pL_d \end{bmatrix} \begin{bmatrix} i_\gamma \\ i_\delta \end{bmatrix} + \begin{bmatrix} -E_x \sin\Delta\theta \\ E_x \cos\Delta\theta \end{bmatrix} \quad (2)$$

Assuming that $p\Delta\theta << \omega_r$, Equation (2) can be expressed as Equation (3).

$$\begin{bmatrix} v_\gamma \\ v_\delta \end{bmatrix} = \begin{bmatrix} R + pL_d & -\omega_r L_q \\ \omega_r L_q & R + pL_d \end{bmatrix} \begin{bmatrix} i_\gamma \\ i_\delta \end{bmatrix} + \begin{bmatrix} -E_x \sin\Delta\theta \\ E_x \cos\Delta\theta \end{bmatrix} \quad (3)$$

The variation of EMF voltage is produced by the position error of rotor ($\Delta\theta$). The error is obtained by using the EMF as Equation (4).

$$\tan\Delta\theta = \frac{\sin\Delta\theta}{\cos\Delta\theta} \quad (4)$$

The discrete equation of extended EMF method is equal to the current model of PMSM as Equation (5), (6).

$$\begin{bmatrix} i_{M\gamma}(n) \\ i_{M\delta}(n) \end{bmatrix} = \begin{bmatrix} 1 - \frac{R}{L_d}T & \omega_M \frac{L_q}{L_d}T \\ -\omega_M \frac{L_q}{L_d}T & 1 - \frac{R}{L_d}T \end{bmatrix} \begin{bmatrix} i_\gamma(n-1) \\ i_\delta(n-1) \end{bmatrix} + \frac{T}{L_d} \begin{bmatrix} v_\gamma(n-1) \\ v_\delta(n-1) \end{bmatrix} - \frac{T}{L_d} \begin{bmatrix} e_{xM\gamma} \\ e_{xM\delta} \end{bmatrix} \quad (5)$$

$$\begin{bmatrix} i_\gamma(n) \\ i_\delta(n) \end{bmatrix} = \begin{bmatrix} 1 - \frac{R}{L_d}T & \omega_r \frac{L_q}{L_d}T \\ -\omega_r \frac{L_q}{L_d}T & 1 - \frac{R}{L_d}T \end{bmatrix} \begin{bmatrix} i_\gamma(n-1) \\ i_\delta(n-1) \end{bmatrix} + \frac{T}{L_d} \begin{bmatrix} v_\gamma(n-1) \\ v_\delta(n-1) \end{bmatrix} - \frac{T}{L_d} \begin{bmatrix} e_{x\gamma} \\ e_{x\delta} \end{bmatrix} \quad (6)$$

Assuming that $\omega_r = \omega_M$, the error between the estimated current from reference model and the real current is described as Equation (7).

$$\Delta e_x = e_x - e_{xM} \quad \Delta e_x = -\frac{L_d}{T}\Delta i \quad (7)$$
$$e_{xM}(n) = e_{xM}(n-1) - K_{ee}\Delta i(n)$$

The extended EMF is estimated in Equation (7), and Fig. 2 and Fig. 3 show the block diagrams of process. Then, $\Delta\theta$ is calculated in Equation (4) by the estimated extended EMF. Finally, the speed and position of rotor are estimated using the PI controller as Equation (8).

$$\omega_M(n) = \Delta\theta_e(n)\left(K_{P\omega} + \frac{K_{I\omega}}{s}\right) \qquad \theta_M(n) = \int \omega_M(n)dt \quad (8)$$
$$\theta_M = \frac{K_{P\omega}s + K_{I\omega}}{s^2 + K_{P\omega}s + K_{I\omega}}\theta \qquad K_{P\omega} = 2\xi_n\omega_{n\omega}, \quad K_{I\omega} = \omega_{n\omega}^2$$

$K_{P\omega}$ and $K_{I\omega}$ are determined by the damping ratio ξ and undamped natural frequency $\omega_{n\omega}$. The estimation of rotor speed and position are obtained by the PI control shown in Fig. 4, and by integrating the output of PI controller, respectively.

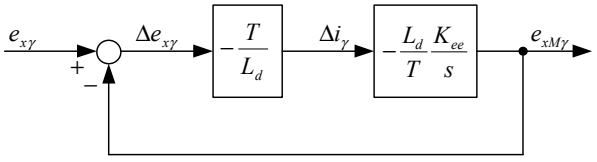

Figure 2. The Estimation of the extended EMF in γ-axis

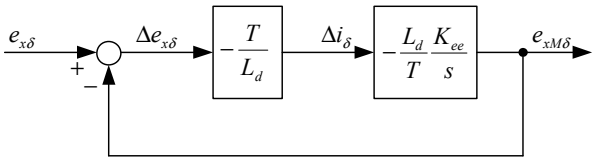

Figure 3. The Estimation of the extended EMF in δ-axis

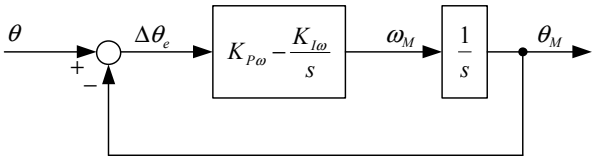

Figure 4. Estimation of the rotor speed in the extended EMF method

B. The High-frequency Injection Method

The extended EMF method in low-speed region including zero speed is not applied in the field, because the EMF is caused in proportion to the rotor speed. In order to supplement this problem, the high-frequency injection method is suggested at low-speed region; including zero speed. Equation (9) is the voltage equation for the IPMSM in the synchronous reference frame.

$$\begin{bmatrix} v_d \\ v_q \end{bmatrix} = \begin{bmatrix} R + pL_d & -\omega_r L_q \\ \omega_r L_d & R + pL_q \end{bmatrix} \begin{bmatrix} i_d \\ i_q \end{bmatrix} + \omega_r K_E \begin{bmatrix} 0 \\ 1 \end{bmatrix} \quad (9)$$

Equation (10) is obtained from Equation (9) by coordinate transformation.

$$\begin{bmatrix} v_\gamma \\ v_\delta \end{bmatrix} = \begin{bmatrix} a_{11} & a_{12} \\ a_{21} & a_{22} \end{bmatrix} \begin{bmatrix} i_\gamma \\ i_\delta \end{bmatrix} + e \begin{bmatrix} -\sin\Delta\theta \\ \cos\Delta\theta \end{bmatrix}$$
$$a_{11} = R + p(L_0 + L_1\cos\Delta\theta) + \omega_r L_1 \sin 2\Delta\theta \quad (10)$$
$$a_{12} = -pL_1 \sin 2\Delta\theta - \omega_r(L_0 - L_1\cos 2\Delta\theta)$$
$$a_{21} = -pL_1 \sin 2\Delta\theta + \omega_r(L_0 + L_1\cos 2\Delta\theta)$$
$$a_{22} = R + p(L_0 - L_1\cos\Delta\theta) - \omega_r L_1 \sin 2\Delta\theta$$
$$L_0 = \frac{L_d + L_q}{2},\ L_1 = \frac{L_d - L_q}{2},\ e = \omega_r K_E$$

Also, Equation (10) is expressed as the state equation with vector form for the current as Equation (11).

$$p\begin{bmatrix} i_\gamma \\ i_\delta \end{bmatrix} = \frac{1}{L_0^2 - L_1^2}\begin{bmatrix} L_0 - L_1\cos 2\Delta\theta & -L_1\sin 2\Delta\theta \\ L_1\sin 2\Delta\theta & L_0 + L_1\cos 2\Delta\theta \end{bmatrix} \quad (11)$$
$$* \left\{ \begin{bmatrix} v_\gamma \\ v_\delta \end{bmatrix} - \begin{bmatrix} R + \omega_r L_1 \sin 2\Delta\theta & -\omega_r(L_0 + L_1\cos 2\Delta\theta) \\ \omega_r(L_0 + L_1\cos 2\Delta\theta) & R - \omega_r L_1 \sin 2\Delta\theta \end{bmatrix} \begin{bmatrix} i_\gamma \\ i_\delta \end{bmatrix} - \omega_r K_E \begin{bmatrix} \sin\Delta\theta \\ \cos\Delta\theta \end{bmatrix} \right\}$$

When the high-frequency sinusoidal voltage ($V_{ac}\sin\omega_{ac}t$) is injected in case of previous defined speed region. Equation (12) is obtained neglecting R=0 and ω_r=0.

$$p\begin{bmatrix} i_{\gamma ac} \\ i_{\delta ac} \end{bmatrix} = \frac{1}{L_0^2 - L_1^2}\begin{bmatrix} L_0 - L_1\cos 2\Delta\theta \\ L_1\sin 2\Delta\theta \end{bmatrix} V_{ac}\sin\omega_{ac}t \ \Leftarrow R = 0, \omega_r = 0 \quad (12)$$

Equation (12) shows that the position error term contains the amplitude of AC component in δ-axis. If the amplitude of AC component in δ-axis ($i_{\delta ac}$) is zero, the position error ($\Delta\theta$) becomes zero. Then, the rotor position can be estimated. $I_{\delta ac}$ can be obtained by FFT. The rotor speed and position can be estimated by Equation (13).

$$I_{\delta ac} = FFT[i_{\delta ac}] = \frac{\omega_{ac}}{2\pi}\int_0^{\frac{2\pi}{\omega_{ac}}} i_\delta \sin\omega_{ac}t\,dt \quad (13)$$
$$\omega_M(n) = I_{\delta ac} K_f\left(K_{P\omega} + \frac{K_{I\omega}}{s}\right) \qquad \theta_M(n) = \theta_M(n-1) + T\omega_M(n-1)$$

In the Equation (13), FFT is calculated by moving average per a period, because the injected frequency is a known parameter. Sometimes, the estimated rotor position at the initial operating has the error of π because the estimated rotor position uses $2\Delta\theta$ in Equation (12). This error is caused by reading the position of N and P-pole in reverse. So, the magnetic polarity is determined after estimating the initial rotor position. Also, Equation (12) is expressed as Equation (14).

$$p\begin{bmatrix} i_{\gamma ac} \\ i_{\delta ac} \end{bmatrix} = \begin{bmatrix} \frac{1}{L_d} \\ 0 \end{bmatrix} V_{ac}\sin\omega_{ac}t \ \Rightarrow pi_{\gamma ac} = \frac{V_{ac}}{L_d}\sin\omega_{ac}t \quad (14)$$

In Equation (14), if a magnetic flux is saturated, it leads to the decrease of L_d and the increase of the amplitude of γ-axis current rapidly. The magnetic polarity can be determined, when the sufficient AC voltages are for magnetic saturation

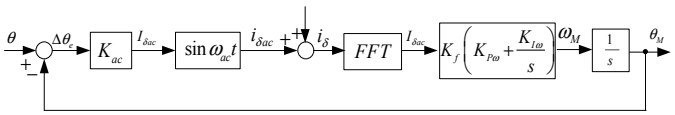

Figure 5. The estimation of speed in the high-frequency injection method

C. Transition Method Between Two Sensorless Algorithms

It is very important smoothly to transit between the extended EMF method and the high-frequency injection method. This paper proposes to apply a hysteresis curve based on the estimated extended EMF $e_{xM\delta}$ of δ-axis with a low-pass filter. In the low-speed region, the high-frequency injection method is applied. Also, the extended EMF is estimated in order to quick transit continuously. The extended EMF $e_{xM\delta}$ is utilized the reference of transition in the hysteresis curve. In Fig. 6, the extended EMF method is applied, if the $e_{xM\delta}$ is more than 30V. Contrary to above situation, if the $e_{xM\delta}$ is less than 20V, the high-frequency injection method is applied sequentially.

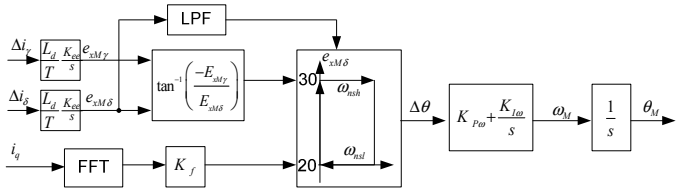

Figure 6. The bock diagram of transition method between two sensorless algorithms

III. VERIFICATION USING EXPERIEMENTS

The proposed method is verified at the Mabuk laboratory, Hyundai Mobis. The IPMSM which is utilized for eco-friendly vehicles is used generally. The position sensor, resolver which has 16 poles is installed in the motor. The motor parameters are shown in Table I. The switching frequency of inverter is 8 kHz.

TABLE I. PARAMETER OF IPMSM

Parameter	Value
Pole	16
Resistance of stator coil (R_s)	13.0 [mΩ]
d-axis inductance of stator (L_d)	330.0 [μH]
q-axis inductance of stator (L_q)	430.0 [μH]
Coefficient of EMF[a]	0.0568 [V·s/rad]

a. EMF(electromotive force)

A. Transition Between Two Sensorless Algoritms

Fig. 7 shows an operating mode conversion between high-frequency injection method in low speed range and extended EMF method in mid-high speed range. Also, it shows a phase

current, real and estimated position during transition from high-frequency injection method to extended EMF method.

The dynamic characteristics of phase current with the high-frequency ripple are shown from the extend EMF method to high-frequency injection method in Fig. 7. The estimated position of rotor is traced the real position to control IPMSM at the moment of transition.

B. Conversion of Operation Mode between Sensored and Sensorless Algorithm

The continuity of the control between sensored and sensorless algorithm is verified at the fail of the position sensor during operation. Fig. 8 shows the performance of operation mode conversion. The sensorless algorithm is not applied during the normal condition of the position sensor.

A phase angle with the estimated position of rotor is applied from the position information of resolver, when the failure is detected the position sensor.

The output torque of IPMSM is 30Nm at 100rpm in Case A; see Fig. 8. The operation of the high-frequency injection method can be shown in Fig. 8. The continuity of control is verified during the mode conversion without dynamic character -istics.

In Case B of Fig. 8 shows the results of the mode conversion at 3000rpm and 30Nm. At this time, the extended EMF method is applied to control the sensorless algorithm, and the continuity of the control can be also verified.

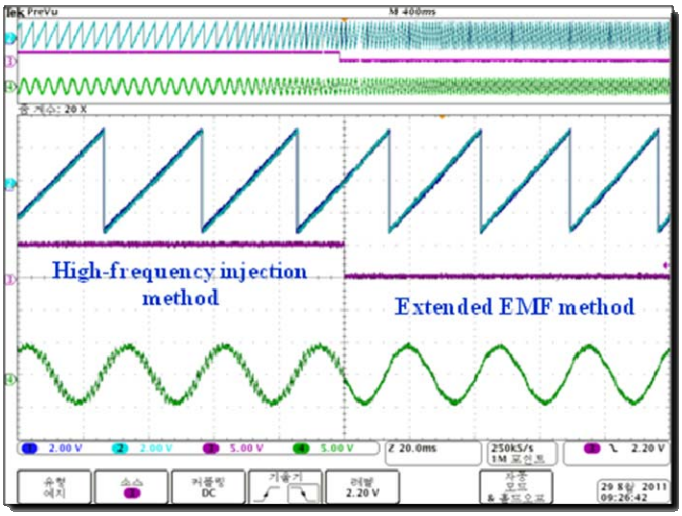

Case A. Transition from high- frequency injection method to extended EMF method

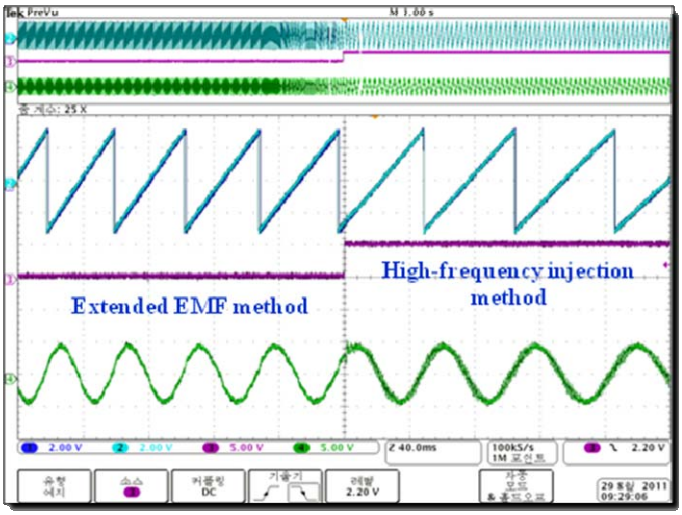

Case B. Transition from Extended EMF method to high-frequency injection method

Figure 7. Transient state characteristics of sensorless control(CH1. Real position, CH2. Estimated position, CH3. Sensorless control mode, CH4. Motor U-phase curent)

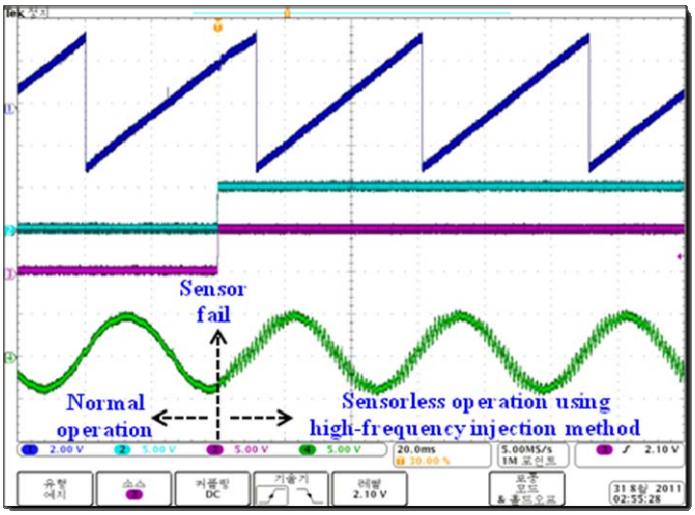

Case A. Conversion to high- frequency injection method sensorless control mode

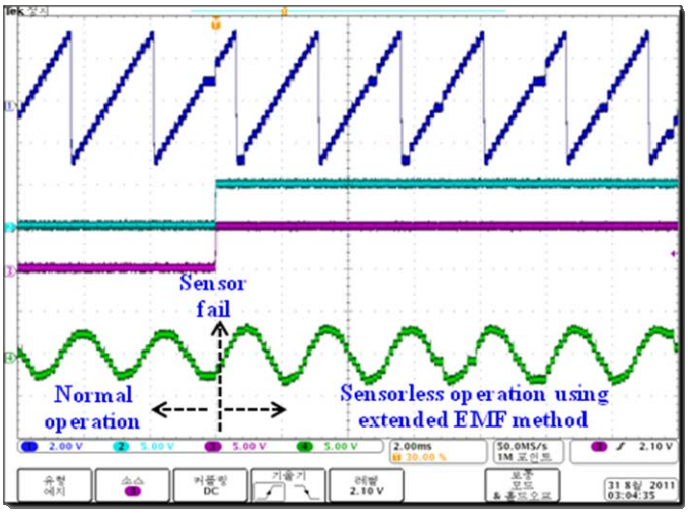

Case B. Conversion to extended EMF method sensorless control mode

Figure 8. Operation mode conversion from sensor control to sensorless control(CH1. Estimated position, CH2. Resolver fault flag, CH3. Sensorless control mode, CH4. Motor U-phase curent)

C. *Comparision of Torque-Speed Characteristics*

The torque-speed curves classified by control mode are shown in Fig. 9. There is torque error at the speed over 3000rpm due to position error, but the magnitude of position error is smaller than the case of 10Nm. From the results of experiment, the backup logic for the control continuity of inverter system can be used using the proposed sensorless algorithm with transition scheme.

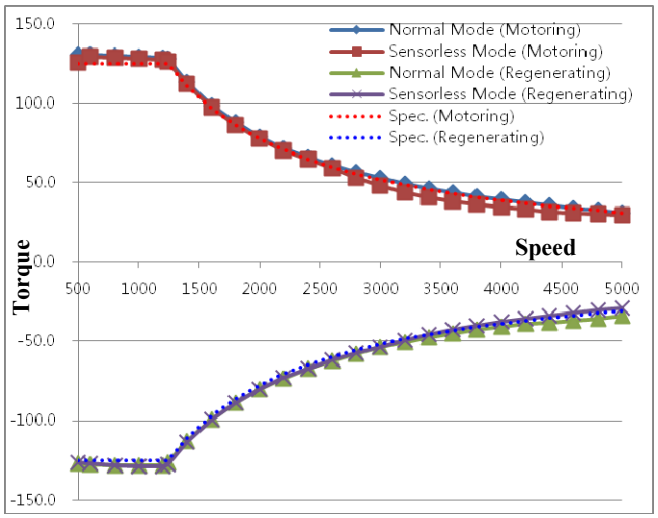

Figure 9. Torque-speed charateristic curve

IV. CONCLUSION

This paper is suggested the sensorless algorithm using the extended EMF method and a high-frequency injection method for eco-friendly vehicle. In the situation of the failure of the position sensor, the proposed sensorless algorithm is applied to a motor control algorithm instead of a real rotor position. The results of experimental show the optimal performance of the proposed sensorless algorithm and the improved responsibility of the sensorless torque control mode in the entire speed region of motor. Therefore, it can be applied enough to secure a fail-safe at the uncertain failure of position sensor, and then the reliability of eco-friendly vehicles can be improved highly.

ACKNOWLEDGMENT

This work was supported in part by the Hyundai Mobis

REFERENCES

[1] N. Matsui, “Sensorless PM Brushless DC Motor Drives,” IEEE Trans. On Industrial Electronics, Vol. 43, no. 2, pp.300-308, 1996.

[2] S. Morimoto, K. Kawamotor, M. Sanada, and Y. Takeda, :Sensorless control strategy for salient-pole PMSM based on extended EMF in rotating reference frame,” IEEE Trans. Ind. Appl., Vol. 38, No. 4, pp.1054-1061, 2002.

[3] S. Ichikawa, M. Tomita, S. Doki, and S. Okuma, “Sensorless control of synchronous reluctance motors based on extended EMF models considering magnetic saturation with online parameter identification,” IEEE Trans. Ind. Appl., Vol 42., No. 5, pp.1264-1274,2006.

[4] Y. Jeong, R.D. Lorenz, T.M. Jahns, and S. Sul, “Initial rotor position estimation of an interior permanent magnet synchronous machine using carrier-frquency injection methods,” IEMDC’03 IEEE International, Vol. 2, pp. 1218-1223, June 2003.